Korean J. Chem. Eng., **27**(5), 1412-1418 (2010)
DOI: 10.1007/s11814-010-0257-9

Carbon nanofibers supported Ru catalyst for sorbitol hydrogenolysis to glycols: Effect of calcination

Long Zhao*, Jinghong Zhou,†, Hong Chen**, Mingguang Zhang**, Zhijun Sui*, and Xinggui Zhou***

*State Key Laboratory of Chemical Engineering, East China University of Science & Technology, 369 Campusbox, Shanghai 200237, P. R. China
**Department of Chemical Engineering, East China University of Science & Technology, Shanghai 200237, P. R. China
(*Received 28 September 2009 • accepted 19 January 2010*)

Abstract−Carbon nanofiber (CNFs) supported Ru catalysts for sorbitol hydrogenolysis to ethylene glycol and propylene glycol were prepared by incipient wetness impregnation, calcination and reduction. The effect of calcination on catalyst properties was investigated using thermal gravimetry analysis, temperature-programmed reduction, X-ray diffraction, X-ray photoelectron spectroscopy, transmission electron microscopy and N_2 physisorption. The results indicated that calcination introduced a great amount of surface oxygen-containing groups (SOCGs) onto CNF surface and induced the phase transformation of Ru species, but slightly changed the texture of Ru/CNFs. The catalytic performance in sorbitol hydrogenolysis showed that Ru/CNFs catalyst calcined at 240 °C presented the highest glycol selectivities and reasonable glycol yields. It was believed that the inhibition and confinement effect of SOCGs around Ru particles as well as the high dispersion of Ru particles was the key factor for the catalytic activity.

Key words: Ru/CNFs Catalyst, Calcination, Sorbitol Hydrogenolysis, Propylene Glycol, Ethylene Glycol

INTRODUCTION

Biomass conversion has received much attention in recent years [1-3]. According to the U.S. Energy Department Report for selecting carbohydrate-derived building blocks in future biorefineries, sorbitol is one of the most potential building blocks, and sorbitol hydrogenolysis to propylene glycol and ethylene glycol affords the opportunity to utilize a renewable resource for the large-scale production of commodity chemicals [4]. Sorbitol hydrogenolysis has been industrialized in China and proved to be environmentally and economically advantageous over traditional petroleum-based glycol production processes.

In the reaction of sorbitol hydrogenolysis to glycols, sorbitol and intermediate species undergo complex reaction pathways including dehydrogenation, retro-aldol condensation, dehydration and hydrogenation. According to the polyol hydrogenolysis mechanism (Fig. 1) proposed by Wang et al. [5], the first step is sorbitol dehydrogenation on metal surface. In a basic environment, dehydrogenated-sorbitol undergoes retro-aldol condensation (C-C bond cleavage reaction) and/or dehydration (C-O bond cleavage reaction), which gives birth to C2 and C3 unsaturated intermediates. Finally, glycols are formed by metal-catalyzed hydrogenation of C2 and C3 intermediates. In addition, if the unsaturated intermediates cannot be hydrogenated over metal catalyst, they will undergo some base-catalyzed by-reac-

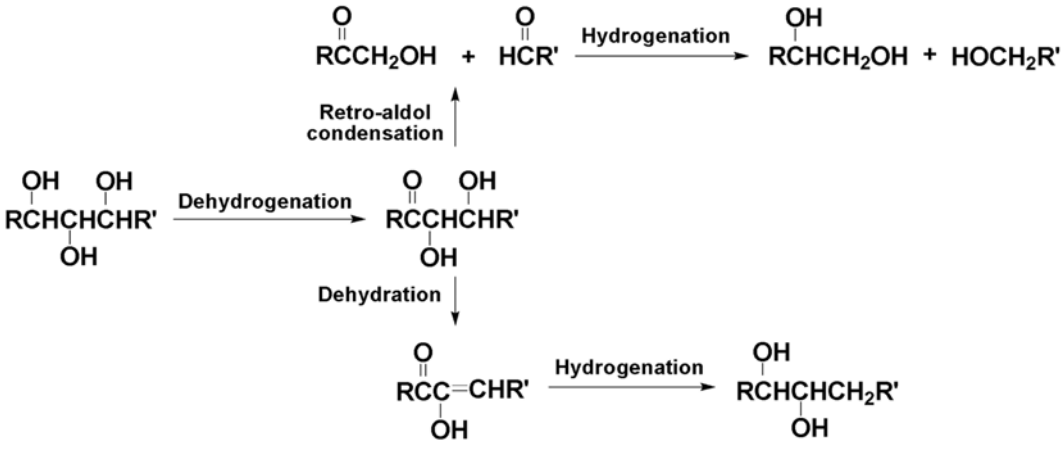

Fig. 1. Polyols hydrogenolysis mechanism proposed by Wang et al. [7].

†To whom correspondence should be addressed.
E-mail: jhzhou@ecust.edu.cn

tions so that glycol selectivities are decreased [5-7]. An overview of previous literature indicates that sorbitol conversion and glycol selectivities depend on the catalyst used in reaction. In our previous work, a novel carbon nanofiber (CNFs) supported Ru catalyst, which was activated by direct reduction, performed much better than commercial Ru/AC catalyst under moderate operating conditions [7]. Besides glycols, some byproducts, such as C1-C4 organic acids, were also detected in the final product mixture. These byproducts are low-value chemicals in comparison with glycols, and their separation is accomplished by energy-consuming distillation process. Undoubtedly, selectivity is a crucial factor for the commercial feasibility of sorbitol hydrogenolysis. Furthermore, higher selectivity to desired product is always pursued in catalysis research, especially in view of sustainable development in recent years [8]. Therefore, it is necessary to conduct further study on Ru/CNFs catalyst for developing a catalyst with higher glycol selectivities under moderate operating conditions.

Recently, the work in our group demonstrated that calcining Ru/CNFs catalyst before catalyst reduction induced some changes in catalyst properties and significantly enhanced glycol selectivities in sorbitol hydrogenolysis. In this paper, we report the corresponding results.

EXPERIMENTAL

CNFs and as-prepared 3.0 wt% Ru/CNFs catalyst were synthesized according to the method described before [7]. Then the as-prepared Ru/CNFs catalyst was calcined for 5 h at 180, 240 and 300 °C, and the calcined catalysts were denoted as Ru/CNFs-180 °C, Ru/CNFs-240 °C and Ru/CNFs-300 °C, respectively. Ru/CNFs catalysts were activated for 5 h at 300 °C in a H_2/Ar (100/300 mL/min) gas mixture before they were used in sorbitol hydrogenolysis.

Thermal gravimetry analysis (TGA) was performed on an SDT Q600 apparatus (TA, USA) using dry air as carrier gas (flow rate: 50 mL/min), and the heating rate was 10 °C/min. N_2 physisorption was conducted on an ASAP 2010 apparatus (Micromeritics, USA) at 77 K after out-gassing the samples for 6 h at 190 °C and 1 mm Hg vacuum. Temperature-programmed reduction (TPR) experiments were carried out on Autochem II 2920 apparatus (Micromeritics, USA). After 1 h of moisture elimination at 150 °C in N_2 atmosphere, the TPR profile of sample was recorded at a heating rate of 10 °C/min in a 10% H_2/Ar mixture. X-ray diffraction (XRD) patterns of Ru/CNFs catalysts were measured on a D/Max2550VB/PC apparatus (Rigaku, Japan) using Cu Kα radiation. Transmission electron microscopy (TEM) was performed on a JSM 2010 apparatus (JOEL, Japan) to observe the microstructure of reduced Ru/CNFs catalysts. Reduced Ru/CNFs catalysts were also characterized by X-ray photoelectron spectroscopy (XPS) on an Axis Ultra DLD apparatus (Kratos, Japan) using Al Kα radiation under 1×10^{-9} Torr, and the binding energy was calibrated by the containment carbon (C 1s=284.6 eV).

Sorbitol hydrogenolysis was performed for 4 h at 220 °C and 10.0 MPa in a 500 mL autoclave (Parr 4575A, USA). The autoclave was charged with 330 g aqueous mixture containing sorbitol (66.00 g), calcium oxide (basic promoter, 10.00 g) and 0.50 g reduced Ru/CNFs catalyst [7]. The liquid product mixture was analyzed on an HPLC system (HP 1100, Agilent, USA) equipped with a Platisil ODS C18 column (4.6 mm×250 mm, 5 μm) and an RID detector.

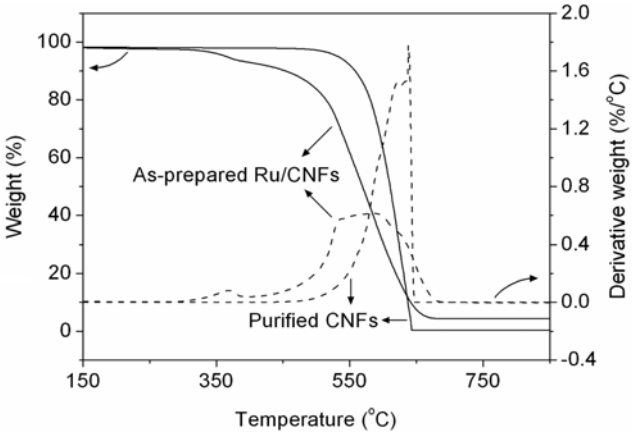

Fig. 2. TGA curves of purified CNFs and as-prepared Ru/CNFs catalyst.

RESULTS AND DISCUSSION

1. Thermal Behavior of Purified CNFs and As-prepared Ru/CNFs Catalyst

TGA was conducted to investigate the thermal stabilities of purified CNFs and as-prepared Ru/CNFs catalyst in air. As shown in Fig. 2, the on-set weight loss temperature (temperature at which 5 wt% weight loss occurred) of purified CNFs was at 530 °C and the CNFs were burnt out at 640 °C. Comparatively, much more weight loss (ca. 27%) was detected for the as-prepared Ru/CNFs catalyst at 530 °C, which clearly indicated that the ruthenium-containing species on CNF surface catalyzed the gasification of CNFs.

To identify whether the catalytic gasification of CNFs took place when the as-prepared Ru/CNFs catalyst was calcined at different temperatures, the samples were accurately weighed before and after calcination. As displayed in Table 1, a significant weight loss (13.33 wt%) was found for Ru/CNFs-300 °C, which was undoubtedly due to the catalytic gasification of CNFs. In the case of Ru/CNFs-180 °C and Ru/CNFs-240 °C, only slight weight losses were detected. Because catalyst had been dried at 120 °C before calcination and $RuCl_3$ easily underwent phase transformation in air [9-11], these slight weight losses should be attributed to the catalytic gasification of CNFs and/or the phase transformation of Ru species.

2. TPR and XRD Characterization

Fig. 3 shows the TPR profiles of $RuCl_3$ precursor and Ru/CNFs catalysts. For the $RuCl_3$ precursor powders, only one broad peak appeared at 217 °C. However, two peaks, which were located at a

Table 1. Catalyst weight loss and Ru loading of the Ru/CNFs catalysts calcined at different temperatures

Catalyst	Catalyst weight loss (%)	Loading[a] (%)
As-prepared Ru/CNFs	-	3.00
Ru/CNFs-180 °C	2.74	3.08
Ru/CNFs-240 °C	3.04	3.09
Ru/CNFs-300 °C	11.33	3.38

[a]The loading was calibrated in consideration of the catalyst weight loss during calcination

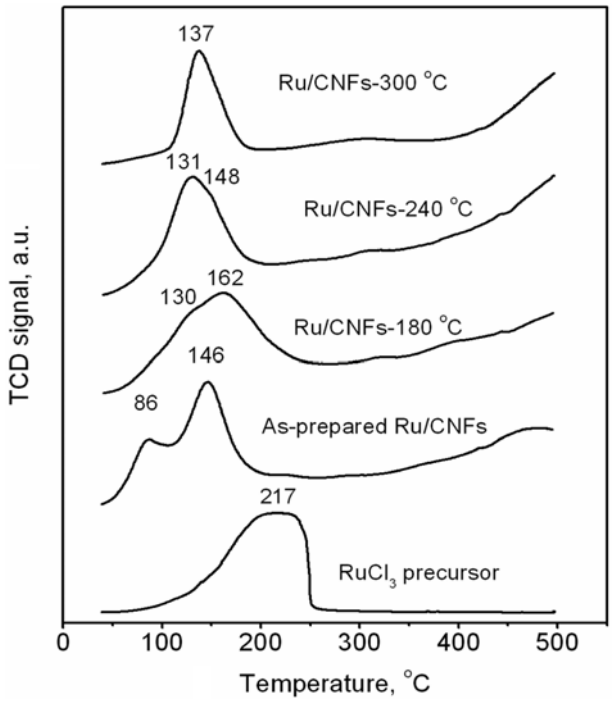

Fig. 3. TPR profiles of $RuCl_3$ precursor and Ru/CNFs catalysts.

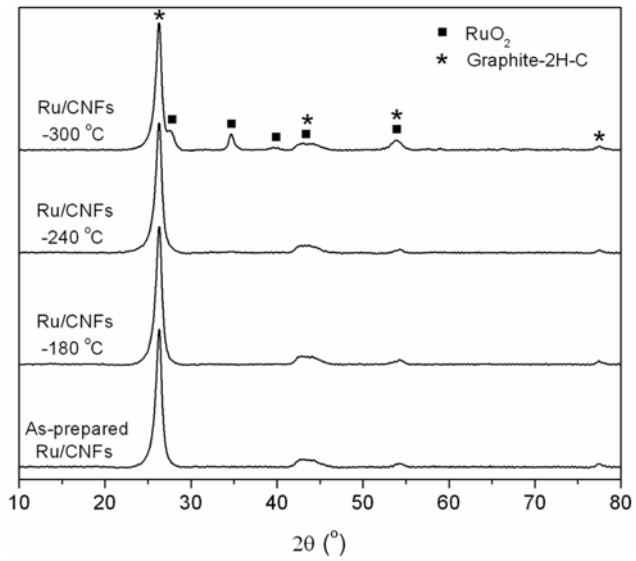

Fig. 4. XRD patterns of Ru/CNFs catalysts.

temperature lower than 250 °C, appeared in the TPR profile of as-prepared Ru/CNFs catalyst. When calcination temperature was increased, the peak at lower temperature became predominant, whereas the one at higher temperature seemed to diminish gradually. As a result, only one peak was observed for Ru/CNFs-300 °C, and it reflected the reduction of RuO_2 particles according to the XRD pattern in Fig. 4. These changes clearly indicated that phase transformation of Ru species took place during catalyst calcination. Additionally, a broad peak was always found at the temperature above 250 °C in the TPR profiles of all the Ru/CNFs catalysts, and it should be attributed to the methanation of carbon atoms [12].

In the TPR profiles of as-prepared Ru/CNFs, Ru/CNFs-180 °C and Ru/CNFs-240 °C, the existence of two peaks at the temperature lower than 250 °C indicated that ruthenium existed in two forms in these three catalysts. It is known that $RuCl_3$ can be oxidized easily and transformed into ruthenium oxychloride ($RuCl_xO_y$) ($0<x<3$, $0<y<2$) or RuO_2 when it is exposed or/and heat-treated in air [9-11]. Therefore, the peak, which was intensified when catalyst calcination temperature was increased, should be ascribed to the reduction process of oxygen-containing Ru species. Accordingly, the peak, which diminished gradually when catalyst calcination temperature was increased, reflected the reduction of $RuCl_3$ species. Although Ru atoms existed in different forms in four Ru/CNFs catalysts, Fig. 3 indicates that reduction at 300 °C could guarantee the activation of these catalysts.

According to the molecule weights of $RuCl_3$ and RuO_2, the catalyst weight loss was supposed to be less than 2.20 wt% even though $RuCl_3$ was completely transformed into RuO_2 during catalyst calcination. As has been discussed above, some Ru atoms still existed in the form of $RuCl_3$ in Ru/CNFs-180 °C and Ru/CNFs-240 °C. Hence the weight losses for Ru/CNFs-180 °C (2.74 wt%) and Ru/CNFs-240 °C (3.04 wt%) indicated that CNFs gasification happened during catalyst calcination.

3. XPS Investigation

As shown in Table 2, calcination increased the amount of surface oxygen-containing groups (SOCGs) on Ru/CNFs catalyst surface, which should be attributed to the gasification of CNFs support during catalyst calcination [13]. For a qualitative analysis, the XPS spectra of O 1s region were deconvolved into five peaks [13-15]: peak 1 (530.6-531.2 eV), carbonyl oxygen of quinines; peak 2 (532.1-532.9 eV), carbonyl oxygen atoms in esters, anhydrides and oxygen atoms in hydroxyl groups; peak 3 (533.4-533.8 eV), non-carbonyl (ether-type) oxygen atoms in esters and anhydrides; peak 4 (534.8-535.1 eV), oxygen atoms in carboxyl groups; and peak 5 (536.2-536.7 eV), adsorbed water and/or oxygen. From the deconvolution results displayed in Table 2 and Fig. 5(a)-(d), one can see that the distribution of SOCGs depended on calcination temperature.

In addition, the less intense Ru 3p region instead of Ru 3d region

Table 2. Surface O 1s atomic concentration in as-prepared and reduced Ru/CNFs catalysts

Catalyst	O 1s atomic concentration, %					
	Sum	Peak 1	Peak 2	Peak 3	Peak 4	Peak 5
As-prepared Ru/CNFs	1.99	0.87	0.47	0.42	0.11	0.12
Ru/CNFs-180 °C	4.31	1.49	0.88	1.53	0.26	0.15
Ru/CNFs-240 °C	4.78	1.38	1.84	0.94	0.38	0.24
Ru/CNFs-300 °C	5.62	2.39	0.52	1.85	0.52	0.35

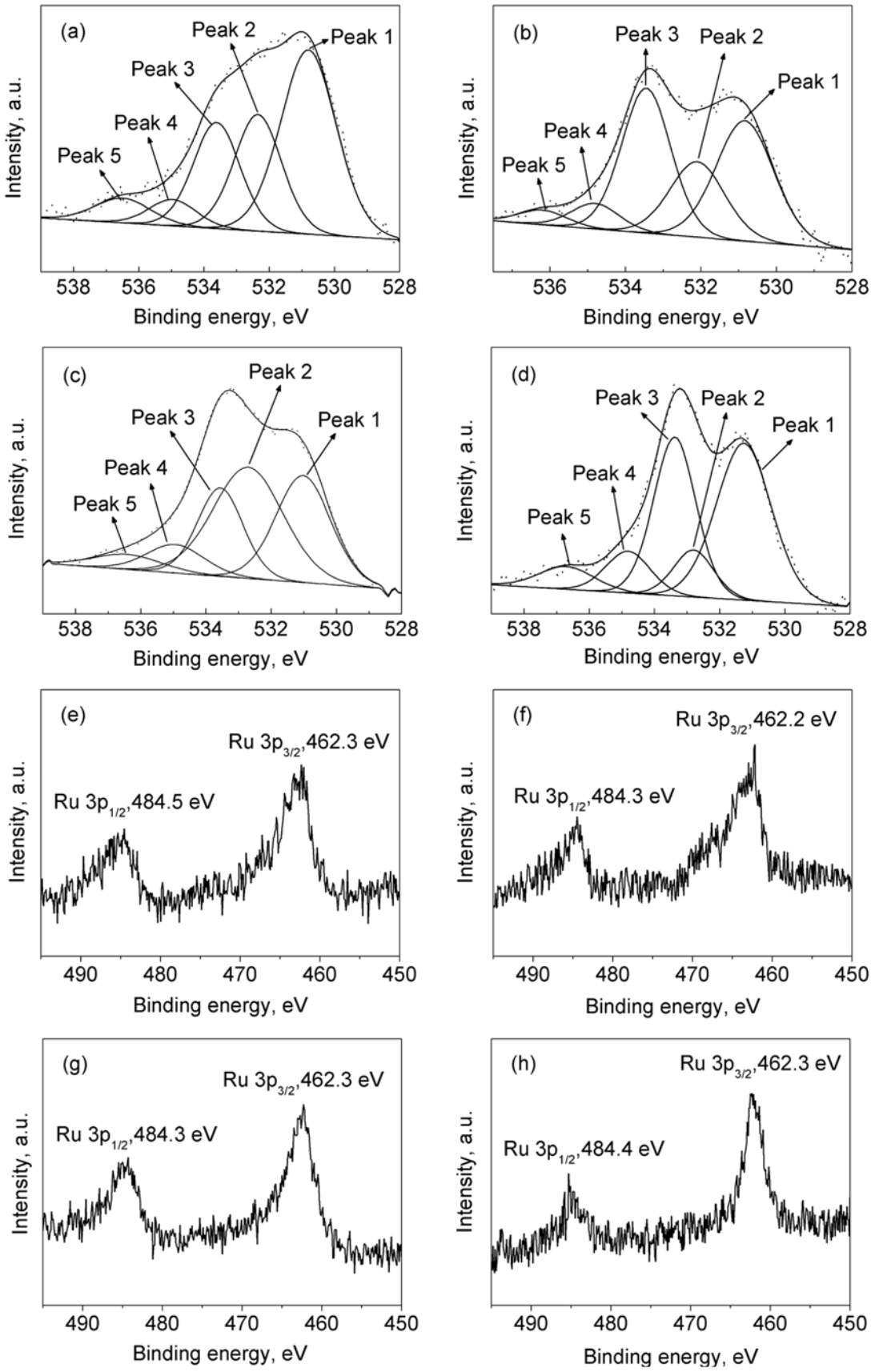

Fig. 5. XPS spectra of the Ru/CNFs catalysts after reduction treatment. (a) O 1s region for as-prepared Ru/CNFs, (b) O 1s region for Ru/CNFs-180 ºC, (c) O 1s region for Ru/CNFs-240 ºC, (d) O 1s region for Ru/CNFs-300 ºC, (e) Ru 3p region for as-prepared Ru/CNFs, (f) Ru 3p region for Ru/CNFs-180 ºC, (g) Ru 3p region for Ru/CNFs-240 ºC, (h) Ru 3p region for Ru/CNFs-300 ºC.

was used to study the chemical state of the Ru particles because of the overlap of Ru $3d_{3/2}$ peak with C 1s region [16,17]. As shown in Fig. 5(e)-(h), the binding energy of Ru $3p_{3/2}$ was 462.2-462.3 eV and the binding energy of Ru $3p_{1/2}$ was 484.2-484.5 eV, which was in agreement with other studies on Ru/CNFs catalysts [18,19] and multi-wall carbon nanotubes (MWCNTs) supported Ru particles [16]. This result indicated that Ru particles existed in approximately identical chemical state in all the reduced Ru/CNFs catalysts, though Ru atoms existed in different forms when the as-prepared Ru/CNFs catalyst was calcined at different temperatures.

4. TEM Observation

As shown in Fig. 6(a)-(c), Ru particles dispersed on CNF surface with almost identical particle size around 1.0 nm in as-prepared Ru/CNFs, Ru/CNFs-180 °C and Ru/CNFs-240 °C, and this result rationalized the fact that XRD technique did not detect any Ru species in these three catalysts. In the case of reduced Ru/CNFs-300 °C catalyst (Fig. 6(d)), Ru particles located on a rough CNF surface with particle size around 10 nm, which reflected the sintering of Ru precursor particles during catalyst calcination at 300 °C. The rough CNF surface in the reduced Ru/CNFs-300 °C catalyst should be related to the significant gasification of CNFs during cal- cination.

5. N_2 Physisorption

In Fig. 7(a), all the isotherms appear as type IV according to the IUPAC classification and evidenced the mesoporous texture of Ru/

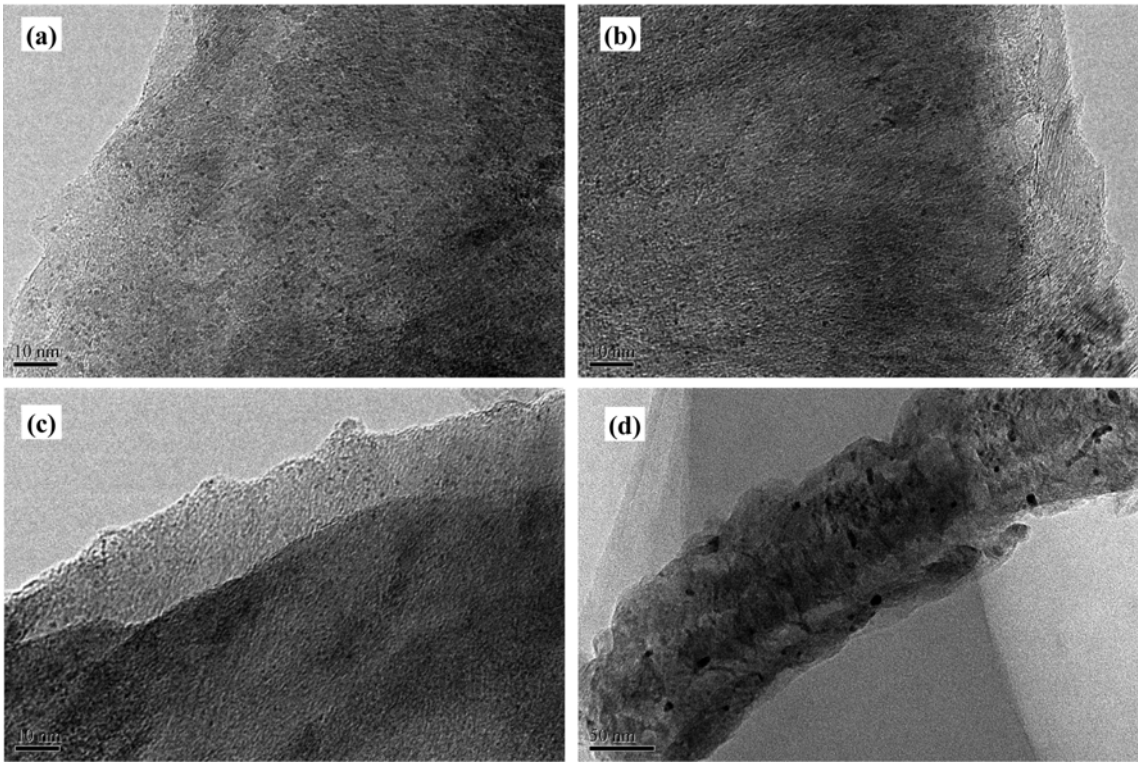

Fig. 6. Typical TEM images of reduced Ru/CNFs catalysts. (a) as-prepared Ru/CNFs; (b) Ru/CNFs-180 °C; (c) Ru/CNFs-240 °C and (d) Ru/CNFs-300 °C.

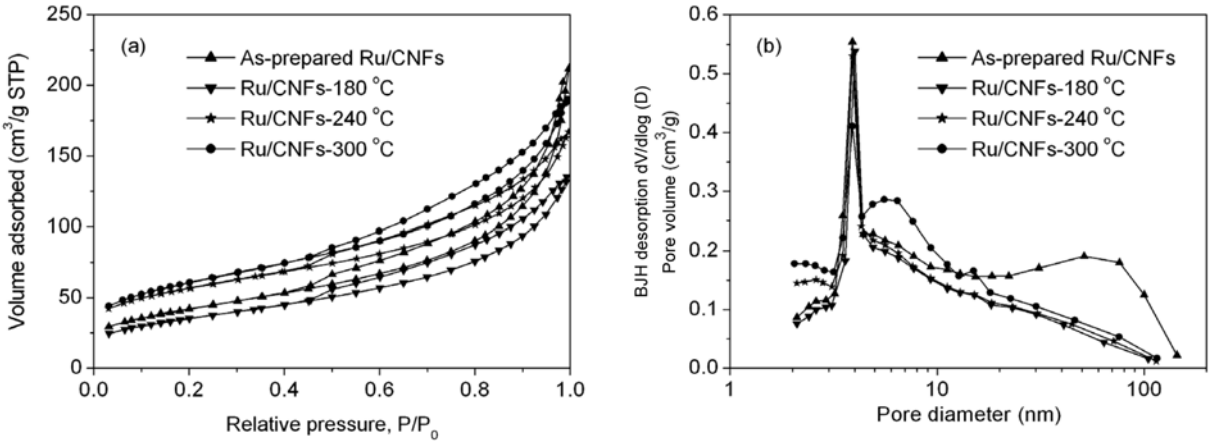

Fig. 7. N_2 adsorption-desorption isotherms (a) and pore size distribution (b) of Ru/CNFs catalysts.

Table 3. Catalytic performance of the Ru/CNFs catalysts in sorbitol hydrogenolysis[a]

Catalyst	Sorbitol conversion (%)	Glycol selectivities (%)			Glycols yields (%)		
		EG	PG	Sum	EG	PG	Sum
As-prepared Ru/CNFs	49.89	20.12	27.35	47.47	10.04	13.64	23.68
Ru/CNFs-180 °C	35.51	24.21	35.51	59.72	8.60	12.61	21.21
Ru/CNFs-240 °C	32.62	25.29	39.75	65.04	8.25	12.97	21.22
Ru/CNFs-300 °C	22.74	10.78	24.34	35.12	2.45	5.53	7.98

[a]EG=ethylene glycol, PG=propylene glycol

CNFs catalysts. The pore size distributions of catalysts are given in Fig. 7(b). For the as-prepared Ru/CNFs, the size of the primary pores was around 3.9 nm, and the size of the secondary pores ranged from 11.2 to 144 nm. Calcination at 180 °C and 240 °C did not alter the pore size distribution around 3.9 nm but clearly decreased the amount of the pores with pore size larger than 11.2 nm. As a result, the BJH desorption average pore diameter was decreased from 8.6 nm to 6.6 nm (Ru/CNFs-180 °C) and to 6.1 nm (Ru/CNFs-240 °C). When the as-prepared Ru/CNFs was calcined at 300 °C, the amounts of the pores with pore size around 3.9 nm and the pores with pore size larger than 11.2 nm were reduced, but more pores with pore size from 4.3 nm to 11.2 nm emerged and resulted in the average pore diameter of 6.2 nm.

6. Sorbitol Hydrogenolysis

Table 3 shows that the catalytic performance of as-prepared Ru/CNFs catalyst was remarkably changed by calcination treatment. Calcining catalyst at 180 °C and 240 °C decreased sorbitol conversion but enhanced glycol selectivities, especially the selectivity to PG. However, both sorbitol conversion and glycol selectivities were remarkably decreased when the as-prepared Ru/CNFs was calcined at 300 °C. Noticeably, by virtue of the higher glycol selectivities, Ru/CNFs-180 °C and Ru/CNFs-240 °C displayed similar glycol yields in comparison with as-prepared Ru/CNFs.

In the point of view of sustainable development and commercial feasibility, Ru/CNFs-240 °C was the best catalyst for sorbitol hydrogenolysis, because it displayed the highest selectivity and reasonable yield. In other words, calcination at 240 °C before catalyst reduction improved the catalytic performance of as-prepared Ru/CNFs by modifying some catalyst properties. As displayed in Table 1 and Fig. 5-6, Ru loading, the chemical state of Ru particles and Ru particle size on CNFs were approximately identical in as-prepared Ru/CNFs and Ru/CNFs-240 °C, so these factors could not explain the effect of calcination on the catalytic performance of as-prepared Ru/CNFs. Although calcination at 240 °C decreased the BJH desorption average pore diameter from 8.6 nm to 6.1 nm, this slight modification could not bring about a remarkable influence on the internal diffusion of the reactants. Thus the variance in pore size distribution should not be considered as the major factor responsible for the observed significant change in the catalytic performance of as-prepared Ru/CNFs, either.

On the basis of sorbitol hydrogenolysis mechanism discussed in the introduction section, it seems that the most proper explanation for the effect of calcination at 240 °C on the catalytic performance of as-prepared Ru/CNFs should be ascribed to the modification to SOCGs. As shown in Table 2, calcination at 240 °C significantly increased the amount of SOCGs, especially carbonyl group and hydroxyl group (peak 1 and 2). Since Ru species particles could catalyze CNF gasification during catalyst calcination, it is believed that SOCGs mainly existed around Ru particles in Ru/CNFs-240 °C. As a result, these polar SOCGs restrained sorbitol molecule from adsorbing on Ru particles via some interactions, such as hydrogen bond and orientation force between SOCGs and the hydroxyl groups in sorbitol molecule. This inhibition effect decreased the rate of sorbitol dehydrogenation, and consequently decreased the sorbitol conversion. Similarly, the SOCGs around Ru particles confined the polar unsaturated species in the vicinity of Ru particles. This confinement effect made the unsaturated species preferentially undergo hydrogenation over Ru particles rather than by-reactions in the bulk liquid phase, so higher glycol selectivities were obtained over Ru/CNFs-240 °C. Although the above effect of SOCGs on sorbitol hydrogenolysis has not been reported in previous studies, researchers have found that the interactions between SOCGs and reactants imposed positive or negative effects on many catalytic reactions, such as cinnamaldehyde hydrogenation over Ru/CNFs and Pt/CNFs [18,20, 21], oxidation of benzyl alcohol over Ru/CNFs [22] and hydrodechlorination of chlorobenzenes over Pd/AC, Pd/graphite and Pd/CNFs [23].

As shown in Table 2, Ru/CNFs-180 °C and Ru/CNFs-240 °C had similar amount of SOCGs after reduction treatment. Furthermore, catalyst characterizations showed that the two catalysts were very similar in terms of Ru loading, pore size distribution and Ru particle size. As a result, they displayed similar catalytic performance in sorbitol hydrogenolysis. Although Ru/CNFs-300 °C had the most amount of SOCGs among four catalysts, it performed worst in terms of sorbitol conversion and glycol selectivities. This was probably because of the much larger Ru particles or lower Ru dispersion in Ru/CNFs-300 °C (Fig. 6). The lower Ru dispersion meant fewer Ru active sites for sorbitol hydrogenolysis and hence lower sorbitol conversion. Moreover, the larger Ru particles were also responsible for the lower selectivity, which has been proven in our other study where the Ru particles around 18 nm over activated carbon displayed very low selectivities in sorbitol hydrogenolysis [7]. As was described in the introduction section, the formation of glycols in sorbitol hydrogenolysis is achieved by metal-catalyzed hydrogenation of unsaturated species [5], so the lower glycol selectivities over the larger Ru particles could be rationalized by the fact that the larger Ru particles were poorly active to hydrogenate unsaturated species [24].

CONCLUSIONS

Carbon nanofiber (CNFs) supported Ru catalyst was prepared and then calcined at different temperatures before reduction treat-

ment. Catalyst weighing, TPR and XRD characterization revealed that catalytic gasification of CNFs and phase transformation of Ru precursor took place during calcination. XPS investigation demonstrated that a large amount of SOCGs were introduced onto the CNFs surface when the as-prepared Ru/CNFs catalyst was calcined. N_2 physisorption showed that the textural structure of the as-prepared Ru/CNFs was slightly altered by calcination. It was found that Ru particles uniformly dispersed on CNFs surface with particle size around 1.0 nm when as-prepared Ru/CNFs, Ru/CNFs-180 ºC and Ru/CNFs-240 ºC were reduced. Comparatively, larger Ru particles around 10 nm were found on the rough CNF surface in the reduced Ru/CNFs-300 ºC.

All the reduced Ru/CNFs catalysts were used in sorbitol hydrogenolysis to propylene glycol and ethylene glycol. It was found that catalyst calcination significantly changed the catalytic performance of as-prepared Ru/CNFs catalyst. Ru/CNFs-240 ºC presented the highest selectivity as well as reasonable glycol yields. Catalyst characterization suggested that the appropriate amount and distribution of SOCGs and the high Ru dispersion should be responsible for the good performance of Ru/CNFs-240 ºC catalyst. Moreover, a model, in which sorbitol hydrogenolysis was influenced by the inhibition effect and the confinement effect of SOCGs around Ru particles, was proposed to explain the role of SOCGs.

ACKNOWLEDGEMENTS

The authors acknowledge the financial support from National Natural Science Foundation of China (No. 20776041) and Ministry of Education of China (IRT0721).

REFERENCES

1. S. W. Lee, S. S. Nam, S. B. Kim, K. W. Lee and C. S. Choi, *Korean J. Chem. Eng.*, **17**, 174 (2000).
2. Z. M. Wang, J. S. Lee, J. Y. Park, C. Z. Wu and Z. H. Yuan, *Korean J. Chem. Eng.*, **25**, 670 (2008).
3. Z. M. Wang, J. S. Lee, J. Y. Park, C. Z. Wu and Z. H. Yuan, *Korean J. Chem. Eng.*, **24**, 1027 (2007).
4. T. Werpy, G. Petersen, A. Aden, J. Bozell, J. Holladay, J. White, A. Manheim, D. Elliot, L. Lasure, S. Jones, M. Gerber, K. Ibsen, L. Lumberg and S. Kelley, U.S. Department of Energy Report (2004).
5. K. Y. Wang, M. C. Hawley and T. D. Furney, *Ind. Eng. Chem. Res.*, **34**, 3766 (1995).
6. M. A. Andrews and S. A. Klaeren, *J. Am. Chem. Soc.*, **111**, 4131 (1989).
7. L. Zhao, J. H. Zhou, Z. J. Sui and X. G. Zhou, *Chem. Eng. Sci.*, **65**, 30 (2009).
8. G. A. Somorjai and R. M. Rioux, *Catal. Today*, **100**, 201 (2005).
9. V. Mazzieri, F. Coloma-Pascual, A. Arcoya, P. C. L'Argentière and N. S. Fígoli, *Appl. Surf. Sci.*, **210**, 222 (2003).
10. P. G. J. Koopman, A. P. G. Kieboom and H. Van Bekkum, *J. Catal.*, **69**, 172 (1981).
11. A. Infantes-Molina, J. Mérida-Robles, E. Rodríguez-Castellón, J. L. G. Fierro and A. Jiménez-López, *Appl. Catal. A*, **341**, 35 (2008).
12. M. Cerro-Alarcón, A. Maroto-Valiente, I. Rodríguez-Ramos and A. Guerrero-Ruiz, *Carbon*, **43**, 2711 (2005).
13. J. H. Zhou, Z. J. Sui, J. Zhu, P. Li, D. Chen, Y. C. Dai and W. K. Yuan, *Carbon*, **45**, 785 (2007).
14. U. Zielke, K. J. Hüttinger and W. P. Hoffman, *Carbon*, **34**, 983 (1996).
15. P. V. Lakshminarayanan, H. Toghiani and C. U. Pittman Jr., *Carbon*, **42**, 2433 (2004).
16. J. X. Pan, J. H. Li, C. Wang and Z. Y. Yang, *React. Kinet. Catal. Lett.*, **90**, 233 (2007).
17. C. Bock, C. Paquet, M. Couillard, G. A. Botton and B. R. Macdougall, *React. J. Am. Chem. Soc.*, **126**, 8028 (2004).
18. M. L. Toebes, F. F. Prinsloo, J. H. Bitter, A. J. vanDillen and K. P. de Jong, *J. Catal.*, **214**, 78 (2003).
19. E. Asedegbega-Nieto, B. Bachiller-Baeza, D. G. Kuvshinov, F. R. García-García, E. Chukanov, G. G. Kuvshinov, A. Guerrero-Ruiz and I. Rodríguez-Ramos, *Carbon*, **46**, 1046 (2008).
20. M. L. Toebes, Y. H. Zhang, J. Hájek, T. A. Nijhuis, J. H. Bitter, A. J. vanDillen, D. Y. Murzin, D. C. Koningsberger and K. P. de Jong, *J. Catal.*, **226**, 215 (2004).
21. M. L. Toebes, T. A. Nijhuis, J. Hájek, J. H. Bitter, A. J. van Dillen, D. Y. Murzin and K. P. de Jong, *Chem. Eng. Sci.*, **60**, 5682 (2005).
22. T. Tang, C. Yin, N. Xiao, M. Guo and F. Xiao, *Catal. Lett.*, **127**, 400 (2009).
23. C. Amorim and M. A. Keane, *J. Chem. Technol. Biotechnol.*, **83**, 662 (2008).
24. A. J. Plomp, H. Vuori, A. O. Krause, K. P. de Jong and J. H. Bitter, *Appl. Catal. A*, **351**, 9 (2008).